A Code for the Preliminary Design of Cooled Supercritical CO_2 Turbines and Application to the Allam Cycle

Scaccabarozzi, Roberto; Martelli, Emanuele; Pini, Matteo; De Servi, Carlo Maria; Chiesa, Paolo; Gatti, Manuele

DOI
10.1115/1.4052146

Publication date
2022

Document Version
Final published version

Published in
Journal of Engineering for Gas Turbines and Power

Roberto Scaccabarozzi[1]
Politecnico di Milano,
Department of Energy,
via Lambruschini 4,
Milan 20156, Italy;
Laboratorio Energia & Ambiente Piacenza (LEAP),
via Nino Bixio 27/C,
Piacenza 29121, Italy
e-mail: roberto.scaccabarozzi@polimi.it

Emanuele Martelli[1]
Department of Energy,
Politecnico di Milano,
via Lambruschini 4,
Milan 20156, Italy
e-mail: emanuele.martelli@polimi.it

Matteo Pini
Propulsion and Power,
Aerospace Engineering Faculty,
Delft University of Technology,
Kluyverweg 1,
Delft 2629 HS, The Netherlands
e-mail: m.pini@tudelft.nl

Carlo Maria De Servi
Flemish Institute for Technological Research (VITO),
Boeretang 200,
Mol 2400, Belgium
e-mail: carlo.deservi@vito.be

Paolo Chiesa
Department of Energy,
Politecnico di Milano,
via Lambruschini 4,
Milan 20156, Italy
e-mail: paolo.chiesa@polimi.it

Manuele Gatti
Department of Energy,
Politecnico di Milano,
via Lambruschini 4,
Milan 20156, Italy
e-mail: manuele.gatti@polimi.it

A Code for the Preliminary Design of Cooled Supercritical CO_2 Turbines and Application to the Allam Cycle

This paper documents a thermo-fluid-dynamic mean-line model for the preliminary design of multistage axial turbines with blade cooling applicable to supercritical CO_2 turbines. Given the working fluid and coolant inlet thermodynamic conditions, blade geometry, number of stages and load criterion, the model computes the stage-by-stage design along with the cooling requirement and ultimately provides an estimate of turbine efficiency via a semi-empirical loss model. Different cooling modes are available and can be selected by the user (stand-alone or combination): convective cooling, film cooling, and thermal barrier coating. The model is applied to attain the preliminary aero-thermal design of the 600 MW cooled axial supercritical CO_2 turbine of the Allam cycle. Results show that a load coefficient varying from 3 to 1 throughout the machine, and a reaction degree ranging from 0.1 to 0.5 lead to the maximum total-to-static turbine efficiency of about 85%. Consequently, as opposed to uncooled CO_2 turbines, a repeated stage configuration is an unsuited design choice for cooled sCO_2 machines. Moreover, the study highlights that film cooling is considerably less effective compared to conventional gas turbines, while increasing the number of stages from 5 to 6 and adopting higher rotational speeds leads to an increased efficiency. [DOI: 10.1115/1.4052146]

1 Introduction

Supercritical CO_2 power cycles have been proposed for low-carbon electricity generation from different primary energy sources: concentrated solar [1,2] and nuclear energy [3], as well as fossil fuels [4], e.g., in place of steam cycles to enhance the efficiency of combined cycle power plants [5], or in oxy-fuel power plants [6] to ease CO_2 capture. Among these applications, oxy-combustion technology recently sparked interest because it has the potential to achieve near-zero or even negative (in case the fuel is biomass) fossil CO_2 emissions with a competitive cost and while producing dispatchable electricity (and cogenerated heat, if required). One intrinsic advantage of the oxy-fuel technologies is related to the semiclosed configuration of the process, which in principle allows for avoiding any form of emission, both CO_2 and pollutants (e.g., NO_x and SO_x) [7].

Among the several oxy-combustion cycles proposed in the literature [8], the Allam cycle is one of the most promising technologies due to the high theoretical efficiency [9], flexibility [10,11], and the envisaged economic performance [12]. It is an intercooled and regenerative semiclosed oxy-combustion power cycle. The working fluid consists of a gas mixture where CO_2 is by far the main component. This is achieved by separating CO_2 from the rest of the combustion products and by recirculating it to a large extent into the combustor to reduce the flame temperature. The Allam cycle inventors claim that it is possible to achieve a net electric efficiency of 58.9% with a specific investment of 800–1000 $\$/kW_{el}$ [13]. However, an independent study performed by the International Energy Agency Greenhouse Gas R&D Program (IEA-GHG) reports an expected efficiency of 55.1% and a specific cost of 1320 $€/kW_{el}$ [12]. These efficiency and cost values, even if less appealing compared to those reported by the

[1]Corresponding authors.

Manuscript received December 3, 2020; final manuscript received July 30, 2021; published online January 3, 2022. Assoc. Editor: Tim Allison.

inventors, remain the most promising in the field of oxy-combustion technology.

The major step in the development of the Allam power cycle has been the construction of a demonstration plant in La Porte, Texas (USA) with the involvement of leading original equipment manufacturers (OEMs) [14]. Notably, Toshiba Corporation in Yokohama (Japan) is manufacturing the combustor and the sCO_2 turbine, while Heatric in Poole (UK) is providing the multiflow heat exchanger which enables heat transfer among multiple process streams, as envisaged for the recuperator of the Allam cycle. The main technical challenges are associated with the high-temperature, high-pressure components of the system, i.e., the turbine, the combustor, and the regenerator. The turbine is particularly challenging to design as it must operate at temperatures exceeding 1350 K with pressure in the order of 30 MPa. To cope with these challenging operating conditions, the turbine features a cooling system and a double casing design. Moreover, the mechanical stress exerted on the blades is significantly higher if compared to that of a conventional gas turbine, as a result of the higher density of the working fluid. This leads to the adoption of blades with a lower aspect ratio (blade height over chord length), as reported in Moroz et al. [15], Zhang et al. [16], and Wright et al. [17]. Mechanical problems also arise from the corrosiveness of the CO_2–H_2O mixture used as working fluid. A protective coating may be needed, as indicated by Sasaki et al. [18] and Wright et al. [17], thus, further complicating the design of the turbine. The design of this component is key for the application also from a thermodynamic point of view. A previous thermodynamic cycle analysis [9] highlighted that the efficiency and power density of the Allam cycle are highly sensitive to turbine aero-thermal performance and cooling requirements. According to the authors, a percentage-point decrease in the turbine polytropic efficiency or in the effectiveness of the cooling system leads, respectively, to a loss of 0.325 and 0.025 percentage points of the cycle conversion efficiency.

In this context, it is apparent that an accurate estimate of the turbine size, cooling requirements, and efficiency is of paramount importance in the preliminary design phase of an Allam cycle power plant, to obtain confidence in the assessment of cycle performance and costs. Furthermore, in the light of the technical challenges previously discussed and of the unconventional operating conditions of the turbine (1350–1550 K and 20–40 MPa) [13], design practices different from those already established for more conventional gas and steam turbines are required to attain high-performance component designs [17]. In spite of this, the current body of literature on the subject of optimal design of sCO_2 turbines is relatively limited, and there are no defined guidelines for the preliminary design of cooled sCO_2 turbines. Most of the works available in the literature focus on uncooled sCO_2 machine and are mainly derived from the study of nuclear or external combustion applications, where the maximum temperatures are limited by the operation of the reactor or by the heat transfer process. For instance, Han et al. [19] study the turbine of a 5 MW_{el} reheated sCO_2 Bryton cycle test loop with a maximum cycle temperature of 873.15 K; Moroz et al. [15] and Zhang et al. [16] perform the design of turbines for nuclear power applications operating at inlet temperatures around 750 K. Even in the studies considering high-temperature machines, as in the work of Schmitt et al. [20], the analysis focuses only on the fluid-dynamic losses and do not deal with the blade cooling requirements in detail.

A second limitation of available works is related to the fact that the main geometric characteristics of the turbine are generally selected based on conventional gas turbine design practice or as a result of a fluid-dynamic optimization (Schmitt et al. [20]). For instance, Han et al. [19] design a two turbine stages, where the flow and load coefficients as well as the reaction degree are fixed, while the solidity and blade profile are determined by a computational fluid dynamics (CFD) based iterative design methodology. A similar approach is followed by Zhang et al. [16] in the design of a single stage sCO_2 turbine. A sensitivity study on the turbine performance with respect to the design variables, including the impact of cooling flows, is presently lacking, thus preventing the assessment of design guidelines for this kind of machines from the results of the studies documented in the literature.

The aero-thermal design of a cooled sCO_2 turbine is inherently a challenging multidisciplinary problem. The main aim of the design process is to maximize the turbine efficiency, considering not only the main flow but also the cooling streams [21], while ensuring the mechanical integrity of both moving and stationary parts [15]. Usually, the process is carried out by means of multidisciplinary models, progressively increasing the level of detail of the analysis: from a conceptual design phase, where first-principle lumped-parameter models complemented by empirical correlations are used, to the three-dimensional steady and unsteady CFD and finite element model analysis in the final design stages. However, especially when a new turbomachine application is of concern, it is necessary to perform preliminary evaluation of the thermodynamic performance of the machine in the early design phases with little prior knowledge and no previous field experience. The availability of accurate lumped-parameter aero-thermo-mechanical models for turbine design and performance assessment is thus essential for preliminary design and instrumental to the next design phases.

Several numerical models have been developed over the years to this purpose for gas turbines, which also allows for an estimate of the cooling flow requirements [22–25]. These models are usually based on the assumption that the working fluid obeys the ideal gas law. Moreover, they often rely on standard geometrical parameters for the blades (e.g., blade solidity and aspect ratio) and stream parameters (e.g., heat transfer coefficient) typical of air-breathing turbines. As a consequence, these models are reasonably not applicable in the design process of cooled sCO_2 turbines, which operate with dense or supercritical flows characterized by very different thermo-fluid-dynamic and transport properties compared to ideal gases.

The methodology proposed in this work uses state of the art Equation of State (EoS) to estimate the thermo-physical properties and calibrated semi-empirical correlations for the transport properties (viscosity and thermal conductivity) for CO_2-rich mixtures. As for loss correlations of stages and fluid-blade heat transfer coefficients, semi-empirical correlations originally derived for conventional turbines are used. In detail, the Traupel loss model [26] are used to estimate the losses of each blade row (stators and rotors) while classic semi-empirical correlations derived for gas turbines [27,28] are used to estimate the blade-fluid heat transfer coefficients.

The main aim of the work is therefore to fill this gap by making the first steps toward the conception of best practices for the optimal preliminary design of cooled sCO_2 turbines. The focus here is mainly on the aero-thermal performance of the turbine, while mechanical aspects are not considered in detail. To this end, the specific objectives of the work are:

(1) The development of a mean-line aero-thermal turbine design model accounting for cooling effects.
(2) The systematic application of the model in order to obtain an efficient preliminary design of the cooled sCO_2 turbine for the Allam cycle.

2 Methodology

The technical literature review shows that the computational models available to perform a preliminary fluid-dynamic design of cooled axial flow turbines may not be particularly accurate for turbines operating with supercritical working fluids, like sCO_2 turbines. The reason thereof is due to the hypothesis that the working fluid can be well described by the ideal gas law and the parameters of the models are calibrated based on that assumption and using data from air-breathing commercial gas turbines. For instance, the so-called continuous expansion model proposed by El-Masri [23] and its implementation in a commercial software [29], the method developed by Chiesa and Macchi [30], and, to a certain extent, the

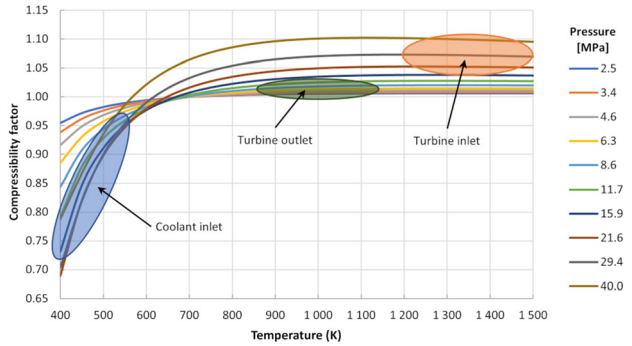

Fig. 1 Compressibility factor (z) of pure CO_2 as a function of temperature (x-axis) and pressure (curves)

methodology described by Jordal et al. [31] and Torbidoni and Massardo [25] are based on the ideal gas model. El-Masri [23] argues that the most critical parameter of the model is the one representing the relative heat to work loading on the machine surface, which highly depends on the stage geometry and its value, without a detailed design of the stage, has to be guessed. As a consequence, the model [29] is only capable to predict the performance of commercially available air-breathing gas turbines while changing the operative conditions. Similarly, in Jordal et al. [31] and Torbidoni and Massardo [25] a semi-empirical correlation, whose parameters are calibrated based on existing gas turbine engines, is used to determine the cooling system performance, and in Chiesa and Macchi [30] the calibration of the cooling system model has been performed by using performance specifications of existing air-breathing gas turbines. Finally, Scaccabarozzi et al. [9] present a 0D model where all the geometrical, thermodynamic (heat transfer), and fluid-dynamic (performance) information, which depends on the actual design of the machine, are modeled by three empirical parameters. Their value is calibrated on the results generated by the in-house code proposed by Chiesa and Macchi assuming ideal gas behavior for CO_2.

The proposed methodology to perform the design of cooled CO_2 turbines combines a blade cooling model together with a mean-line code for estimating the main geometrical parameters of the turbine and the fluid-dynamic losses along the expansion process. Notably, the two models are solved in sequence. First, a preliminary sizing of the expander blade geometry is performed by assuming an uncooled expansion. Then, the blade cooling model uses the output of the mean-line code to evaluate the cooling losses and the required coolant mass flowrate. The only geometrical parameter that is modified during the blade cooling simulation is the trailing edge blade span, which is reduced to account for the lower fluid mass flowrate through the blade cascades with respect to the uncooled turbine. The adaption of the blade height is limited to a few percentage points of the value estimated for the uncooled expansion. The consequent reduction in the blade aspect ratio (i.e., blade height over chord length) has, thus, negligible impact on the loss coefficient predicted by the loss model of the mean-line code in the first step of the methodology.

2.1 Supercritical CO_2 Non-Ideal Gas Effects. The streams evolving within sCO_2 turbines span a range of different thermodynamic conditions and, in some cases (e.g., coolant inlet and turbine inlet streams), their thermo-physical behavior can be significantly different from an ideal gas mixture, therefore requiring the adoption of a more accurate EoS, such as the GERG model [9]. Figure 1 shows the evolution of the compressibility factor of pure CO_2 as a function of temperature and pressure and indicates the conventional operating zone for the sCO_2 turbine featured in the Allam cycle. The outlet conditions are relatively close to the ideal behavior with a compressibility factor (z) only a few percentage points (e.g., 1–3%) higher that one. On the other hand, due to the high inlet pressure, the compressibility factor at the turbine inlet is usually in the range 1.05–1.10, indicating a not negligible discrepancy from the ideal gas behavior (which features $z = 1$ by definition). However, the stream mostly deviating from the ideal gas behavior is the coolant stream, which can have a compressibility factor as low as 0.70, characterized by a significant dependence on the temperature (i.e., steep curves in Fig. 1) compared to the trend of the main stream (horizontal curves in Fig. 1). As a reference, in a conventional gas turbine, the discrepancy of the compressibility factor from one is always lower than 1.5%.

2.2 Fluid-Dynamic Model. The preliminary design of the sCO_2 turbine analyzed in this study has been carried out by using an in-house mean-line model coded in FORTRAN named ZTURBO [32,33], where the working fluid can be arbitrarily selected. More in detail, ZTURBO is linked to an external library [34] allowing one to calculate the calculation of thermodynamic and transport properties of several fluids and mixtures. The library implements a variety of thermodynamic models, such as the GERG-2008 [35] EoS, which is suitable to model the thermodynamic properties of the CO_2-rich mixtures of the Allam cycle, as previously proven in Scaccabarozzi et al. [9] against experimental data. A summary of the input/output variables of ZTURBO is reported in Table 1.

Initially, the stator outlet conditions of the first stage are computed based on the imposed pressure ratio and reaction degree assuming isentropic expansion. The calculation procedure continues with the number of blades according to the Zweifel criterion [36], as reported in Eqs. (1) and (2).

$$\frac{p_b}{c_a} = C_Z \frac{(p_{t,i} - p_{s,ouc})\frac{r_{m,i}+r_{m,ouc}}{2}}{\frac{\rho_i v_{a,i} + \rho_{ouc} v_{a,ouc}}{2}\frac{r_{m,i} v_{t,i} - r_{m,ouc} v_{t,ouc}}{2}} \tag{1}$$

$$N_b = \text{round}\left(\frac{2\pi \frac{r_{m,i}-r_{m,ouc}}{2}}{p_b}\right) \tag{2}$$

where p_b is the blade pitch, c_a is the axial chord length, and N_b is the number of blades. C_z is the Zweifel load coefficient, which is

Table 1 ZTURBO input/output variables

Input	Output
• Number of stages	• Overall power production
• Ratio between the blade height and the mean diameter at the turbine inlet	• Global total-to-total and total-to-static efficiency
• Load coefficient of the first stage	• Specific (to the inlet mass flow rate) power production
• Rotational speed	• Thermo-physical properties at each blade row outlet
• Total-to-static pressure ratio of each stage, excluding the last one	• Velocity triangle of each stage
• Reaction degree of each stage	• Power production of each stage
• Radial evolution of the stage, i.e., rm,ouc/rm,i = 1.0175	• Total-to-total and total-to-static efficiency of each stage
• Axial cord length of each blade row	• Load and flow coefficient of each stage
• Outlet geometric angle of each blade row	• Inlet and outlet blade height and mean diameter of each blade row

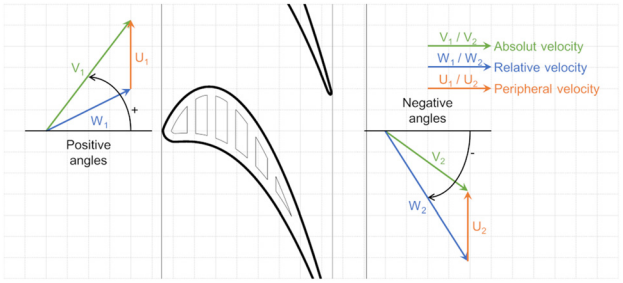

Fig. 2 Illustration of the flow angle convention

fixed at 0.85 in the study and its optimal value can vary for highly loaded stages or, in general, with stage compressibility effects. However, in the absence of openly available design guidelines for cooled turbines, we decided to stick on the value typically referenced in turbomachinery textbooks [37], while the effect of the solidity on turbine performance will investigate in a future work. p_t and p_s are, respectively, the total and static pressure, r_m is the mean diameter radius, ρ is the density, while v_a and v_t are the axial and tangential components of velocity, respectively. Finally, the subscripts i and ouc indicates the inlet and the outlet conditions in the case of no cooling flow.

The mean diameter of the first stage is evaluated given the rotational speed, and the definition of the load coefficient, under the assumption that the Euler work is equal to the isentropic work of the stage. After this step, the main geometrical parameters of the first blade cascade are known, and, hence, it is possible to determine the loss coefficient. To this purpose, the loss model proposed by Traupel [26] is used. Such an empirical model accounts for profile, secondary, and tip. These loss sources are estimated given the blade solidity, aspect ratio, incidence and deflection (flow turning) angles, and Reynolds and Mach numbers. Note that the Traupel's loss model is usually applied to predict the efficiency of large size axial turbines, but its range of applicability (with Mach number in the range 0.1–2.0, blade row inlet and outlet angles, defined as illustrated in Fig. 2, respectively, from –1.05 rad (–60 degree) to 1.05 rad (60 degree) and from –0.25 rad (–14 degree) to –0.80 rad (–45 degree), and trailing edge thickness over pitch ratio between 0.04 and 0.2), makes it suited also for small and medium size turbines.

Once the loss coefficient is known, the actual flow velocity downstream of the cascade is computed, the thermo-physical fluid properties are determined, and the blade span is eventually calculated through the continuity equation. The entire process is iteratively repeated until convergence.

The same procedure is adopted for the rotor design and in turn for all the subsequent stages. Notice that the mean diameter of each new turbine stage is determined based on the dimensionless radial evolution parameter defined in Table 1.

2.3 Blade Cooling Model. A blade cooling model has been implemented in ZTURBO to estimate the coolant requirement for each blade row and its impact on the efficiency of a turbine stage. The cooling model is an extension of the one proposed by Horlock et al. [24] for conventional gas turbines, which enables to consider three different cooling techniques: convective cooling, film cooling, and thermal barrier coating (TBC). This model was calibrated based on experimental data available in the open literature for air-breathing gas turbines. Thus, the validity of the empirical correlations adopted for estimating the heat transfer coefficient of the bulk flow across a blade cascade (see Eqs. (A10) and (A11)), and the film cooling effectiveness (Eq. (A12)) has to be assessed for supercritical CO_2 turbines. However, as there are no experimental data for this kind of application, ad hoc CFD studies are required, which are out of the scope of the present work and that can also be affected by uncertainty.

A schematic representation of the model developed in this work is depicted in Fig. 3. The model requires several input variables,

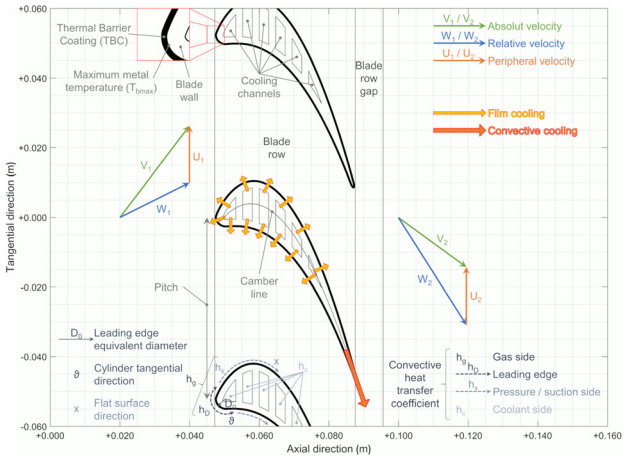

Fig. 3 Schematic of the blade cooling model from the blade channels to the mixing process occurring downstream of the blades (blade-to-blade plane)

concerning the blade material and coating, i.e., the thermal conductivity of the blade metal (k_{bw}) and TBC (k_{TBC}), the thickness of the blade wall (t_{bw}) and TBC (t_{TBC}), as well as concerning the blade geometry, i.e., the ratio between the cooling channel hydraulic diameter ($D_{H,c}$) and the camber line length, the fraction of the coolant used in the film cooling (r_{fc}), the coolant injection angle (α_{ic}), and the interference factor of the cooling channels (I_f).

The five main assumptions underlying the model are:

- Heat losses, either conducted across the shaft or lost from the casing to the outside environment, are assumed to be negligible compared to the gross power output of the turbine. This assumption is appropriate for large scale ("high flow") turbines, differently from radial small-scale turbine which are usually uncooled [38].
- The model computes only the flow required for blade cooling and not those required for disks and case cooling and sealing.
- The blade wall underneath the TBC has a homogeneous temperature equal to the maximum allowable metal temperature (T_{bmax}) assumed in the design.
- The direction of the working fluid velocity, as computed by the uncooled expansion, is not influenced by the injection of the coolant (i.e., the absolute flow angle downstream of the stator and the relative flow angle downstream of the rotor, calculated with respect to the axial direction does not change due to the injection of the cooling flow and it is estimated by preliminary calculations assuming an uncooled expansion process).
- As the assessment of the gas-side convective heat transfer coefficient is concerned, the blade is divided in three main sections: the leading-edge region, the pressure side and the suction side. According to Simon and Piggush [27], the leading edge region can be approximated as a cylinder and the pressure and suction side as flat surfaces. Although no previous work proves the accuracy of the classic blade-fluid heat transfer correlations to supercritical CO_2 flows, being non-dimensional correlations, their possible extension should be guaranteed within the same range of non-dimensional flow numbers (Reynolds, Prandtl, specific heat capacity ratio and Mach). In any case, shall future studies unveil the need of developing more accurate blade-fluid heat transfer coefficients (e.g. correlations accounting for the detailed geometry of the blade profiles and cooling techniques used in supercritical CO_2 turbines), these new correlations could be easily included in the code.

A detailed description of the equations of the model and convergence algorithm is reported in the Appendix.

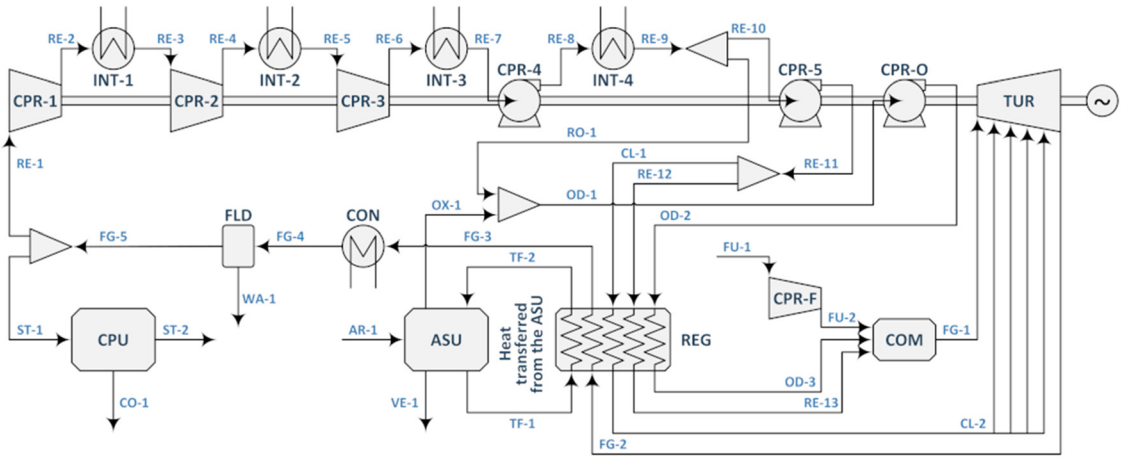

Fig. 4 Simplified process flow diagram of the Allam cycle

3 Case Study

As case study, the developed turbine design methodology has been applied to design a cooled axial turbine for the Allam cycle optimized in Scaccabarozzi et al. [9]. The Allam cycle is an intercooled, regenerative, semiclosed oxy-combustion cycle, which recycles a CO_2-rich mixture to moderate the flame temperature. Its simplified process flow diagram is reported in Fig. 4. The CO_2-rich mixture in RE-1 undergoes intercooled compression above its critical pressure (7.377 MPa for pure CO_2), such that the high density reached at the exit of the intercooler INT-3 allows reducing the power consumption of the compression up to the maximum cycle pressure. After INT-3, the working fluid is split in three streams:

- RO-1 is mixed with the compressed oxygen stream (OX-1) made available by an air separation unit (ASU) to make oxidant stream (OD-1).
- RE-12 is the combustion temperature moderator.
- CL-1 is the turbine (TUR) coolant.

All the streams are compressed and preheated in the regenerator (REG). The oxidant (OD-3) and the temperature moderator (RE-13) are fed to the combustor (COM) with the fuel (FU-1). The flue gas (FG-1), mainly a mixture of CO_2+H_2O, is expanded to generate power in a cooled turbine (TUR) and then flow through the hot side of the regenerator (REG) to provide heat to the cold streams. If needed, part of the low-temperature heat in the regenerator can be provided by the compression section of the ASU. Finally, the flue gas is cooled down close to ambient temperature in a condenser (CON) and the condensed water, generated from the combustion of the fuel, is separated in a knock-out drum (FLD). Most of this flow (e.g., 95%), composed of almost pure CO_2, is recycled back to the intercooled compressor, while the remaining part (ST-1) is purified, if required, and compressed in a CO_2 compression and purification unit (CPU) and sent to the storage.

For the case study, the operative conditions and the composition of the turbine working fluid are reported in Table 2.

The coolant temperature is lower compared to conventional gas turbine; however, the il value is derived from the optimization of the thermodynamic cycle and particularly from the heat recovery process performed within the regenerator (further details about this optimization of the Allam cycle are in [9]). Such, low temperature may result in thermal stress in the blade wall and ultimately its value should be derived from a simultaneous optimization of the thermodynamic cycle and turbine design, while considering the mechanical stress evaluation. However, such analysis is outside of the scope of this work.

Table 3 reports the list of alternative designs of the Allam cycle turbine that have been analyzed. In the cases from 1 to 7, the assumed rotational speed is 3600 RPM, and both 5 and 6 total number of stages have been considered. The selection of the number of stages resulted from a preliminary exploration of the design space of the machine, to ensure acceptable blade heights in the first stator and that the outlet Mach number of the stages were

Table 2 Operative conditions and working fluid composition at turbine inlet

Parameter	Unit of measure	Value
Inlet mass flow rate	kg/s	1214.38
Total inlet pressure	MPa	30.70
Total inlet temperature	K	1427.27
Total outlet pressure	MPa	3.06
Coolant inlet temperature	K	429.63
Maximum blade metal temperature	K	1133.15
Maximum turbine outlet temperature[a]	K	998.15
Expected power output	MW	626.77
Molar composition		
CO_2	$\%_{mol}$	93.14
H_2O	$\%_{mol}$	5.00
N_2	$\%_{mol}$	1.12
Ar	$\%_{mol}$	0.54
O_2	$\%_{mol}$	0.20

[a]Due to the mechanical limitation on the regenerator inlet temperature [14].

Table 3 Design options assessed in the study. These differ for the values assumed for the following design variables: the reaction degree, that is the ratio between the stator and the stage total-to-static enthalpy drop; the load coefficient, which is the ratio between the total-to-total enthalpy drop and the rotor inlet peripheral speed squared; the flow coefficient, that is the ratio between the absolute axial at the outlet and the rotor inlet peripheral speed.

Case no.	Rotational speed (RPM)	Reaction degree	Load coefficient	Flow coefficient
1	3600	0.5	2.5	0.6
2	3600	0.5	2.0	0.6
3	3600	0.5	2.5	0.9
4	3600	0.5	2.0	0.9
5	3600	0.1–0.5	2.5	0.6
6	3600	0.5	3.0–1.0	0.6
7	3600	0.1–0.5	3.0–1.0	0.6
8	7200	0.5	3.0–1.0	0.9
9	7200	0.5	3.0–1.0	0.9

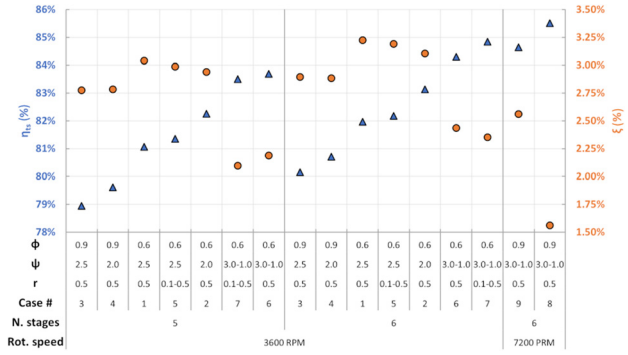

Fig. 5 Summary of the total-to-static overall efficiency (triangles) and the ratio between the coolant and gas inlet mass flowrate (circles) of the 5- and 6-stage designs

within the limits for transonic turbines [39]. The stage count ended up to be higher if compared to an air-breathing gas turbine with the same pressure ratio (e.g., 4-stage turbine), as a consequence of the higher density of the working fluid at the inlet of the sCO_2 turbine. A reduction in the number of stages may be achieved by increasing the power extraction per stage, e.g., by adopting a higher peripheral velocity. However, as the rotational speed is fixed, this would lead to a larger mean diameter with a consequent decrease of the blade height, which, in turn, causes an increase of the secondary losses (smaller h/D_m ratio) and thus a lower turbine performance. Insufficient blade heights may occur in the first stage of the machine. To prevent such a situation, a minimum value for the ratio between the first stage blade height and mean diameter is assumed, which is equal to 0.05 for the cases 1–7 and equal to 0.1 for the other ones.

As far as the other design variables are concerned, in the cases from 1 to 4, the duty coefficients are assumed the same for all the stages, in analogy with the repeating-stage design approach typical of gas turbines. The value of the load coefficient and/or the reaction degree are, instead, varied along the turbine in the cases from 5 to 9. Notice that in case 8 and 9 a rotational speed of 7200 RPM is considered for a 6-stage turbine configuration. The axial chord length have been fixed at 40 mm, while assuming a Zweifel coefficient (Eq. (1) of 0.85 according to gas turbines common design practice [40]. Only in case 9, where the rotational speed of the machine is 7200 RPM, the axial chord length is increased to 60 mm and the Zweifel coefficient is reduced to 0.65, so as to assess the penalty in the turbine performance in the case the mechanical stresses need to be reduced due to the higher centrifugal forces. Similarly, the mean diameter of the blade rows is assumed to increase linearly along the expansion process, as in gas turbines [30]. This increases by 3.5% per stage in the case the rotational speed is 3600 RPM, while by 7.0% for the 7200 RPM designs. It follows that the last stages, whose mechanical design is less challenging as the operating temperature is lower, are characterized by a larger peripheral velocity and thus a higher power extraction. Furthermore, due to the high volumetric ratio of sCO_2 turbines (i.e., ratio between outlet and inlet volumetric flowrate), the higher mean diameter prevents an excessive increase of the blade height of the last stages, which could lead to an increase in profile losses (i.e., high h/D_m ratios).

According to the OEM realizing the turbine of the Allam cycle demonstration plant [13], the adoption of film cooling is not needed given the envisaged inlet turbine conditions if a TBC layer is applied to the blade surface. Furthermore, preliminary calculations reported in [39] show that film cooling is less effective in sCO_2 turbines if compared to air-breathing turbines, due to the higher density and thus Reynolds number of the flow, which promote the mixing of the thin protective film with the main stream. However, even if less effective, due to the relatively high turbine inlet temperature of the selected case study, the authors decided to consider the application of film cooling on the blades of the first stage. A TBC of 0.2 mm thickness, as in gas turbines, is used on the first 3 or 4 stages, respectively, when the machine has a total of 5 or 6 stages. For the last two stages of the turbine, only the adoption of convective cooling is considered given the lower temperature of the fluid. Actually, it may occur that the flow bulk temperature is lower than the maximum allowed metal temperature, thus making cooling un-necessary.

Finally, it is assumed that all the turbine designs feature an outlet diffuser characterized by a semi-opening angle of 0.175 rad (10 degree) and a length of 1 m [41]. Thus, once the outlet geometry of the last stage is known (i.e., mean diameter and blade height) from the design model, it is possible to compute the cross-sectional area ratio (outlet/inlet) of the diffuser and then its efficiency according to the experimental data reported in [42]. Only the axial component of the outlet velocity is recovered, while it is assumed that the tangential component is completely dissipated by viscous effects.

For each case, the thermo-fluid-dynamic performance of the expander is assessed in relation to the reversible power of the streams entering the turbine, coolant included. For the uncooled stages, the efficiency corresponds to the conventional total-to-total enthalpy variation. For a cooled stage, the efficiency is calculated by dividing its actual power output by the power produced by a reversible adiabatic device which mixes and expands the streams up to the stage outlet pressure, according to Eq. (3) [43].

$$\eta_{ad,tt} = \frac{\dot{W}_{blade}}{\dot{m}_g\left(h_{t,g,i} - h\left(p_{t,g,o}, \frac{\dot{m}_g s_{g,i} + \dot{m}_c s_{c,i}}{\dot{m}_g + \dot{m}_c}\right)\right) + \dot{m}_c\left(h_{t,c,i} - h\left(p_{t,g,o}, \frac{\dot{m}_g s_{g,i} + \dot{m}_c s_{c,i}}{\dot{m}_g + \dot{m}_c}\right)\right)} \tag{3}$$

Notice that, for the sake of simplicity, in the analysis the composition of the main stream and coolant is the same, otherwise, the computation of the outlet gas entropy would be also affected by the variation of the fluid composition.

4 Results

Figure 5 shows a summary of the overall total-to-static efficiency and the ratio between the coolant and gas inlet mass flow rates for the analyzed designs. Generally, the coolant requirement is significantly smaller compared to air-breathing gas turbines because the most critical stages (the first and the second ones) have a small volumetric flowrate due to the high density of the working fluid, thus, the metal surface that has to be cooled, comprehensive of blades and end-walls, is comparatively reduced is about 16%, while for the designs of the case study considered it varies between a minimum of 0.9% for case 4 of the 5-stage design to a maximum of about 1.4% for case 5 of the 6-stage design. It has to be pointed out that the significant reduction of coolant requirement is also related to two other major factors: the

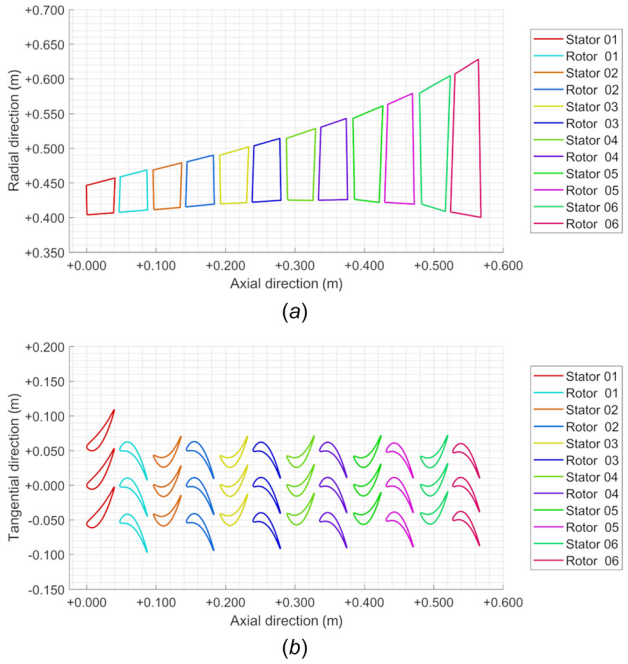

Fig. 6 6-Stage case 1 design (reaction degree 0.5, load coefficient 2.5, flow coefficient 0.6): (*a*) cross-sectional view of the machine, (*b*) midspan blade-to-blade profile

gas inlet temperature is significantly lower for the sCO_2 turbine, and the cooling flow has lower temperature and higher heat capacity (c_p). Indeed, for the SGT5-4000F, the gas inlet temperature is 1704 K, the coolant inlet temperature is 679 K and the constant pressure heat capacity is 1.1 kJ/kgK, whereas for the turbine of the Allam cycle, the same properties are, respectively, 1427 K, 430 K and 1.8 kJ/kgK. In this case, the reported value for the film cooling effectiveness is around 9% for both the first stator and rotor, and this value is significantly lower compared to the one of the SGT5-4000F, i.e., 20%.

Generally, the mean radius at the turbine inlet is in the range of 0.47–0.54 m and 0.42–0.49 m, respectively, for the 5-stage and 6-stage turbine; similarly the inlet blade height varies between 47–54 mm and 42–49 mm (fixed inlet h/D_m ratio at 0.05). The geometry of the turbine first stages is similar to that of a high-pressure stage of a steam turbine due to the high density of the working fluid. On the other hand, the mean radius and blade height at the turbine exit are in the ranges 0.55–0.64 m and 112–200 mm for the 5-stage configuration and between 0.51–0.60 m and 128–230 mm for the 6-stage cases. The geometrical ratios of the last turbine stage are closer to those of a conventional gas turbine. This peculiar change in geometry is typical of sCO_2 turbine, which usually operates with high volumetric ratio. For instance, in this case, the ratio between the outlet and inlet volumetric flowrate is around 7, which is three times higher than that of a steam turbine with the same inlet conditions (T,p) and power output. For instance, Fig. 6 depicts the cross-sectional view and the midspan blade-to-blade profile of the 6-stage design of case 1.

The consequences of the working fluid nonideal behavior, especially of the coolant, are shown in Table 4, which compares the model results of case 1 with the GERG-2008 EoS or considering the working fluid as an ideal gas mixture. The most significant change is the increase of the cooling flow requirement of 16.5 kg/s, corresponding to a relative increase of 42% points. This difference is mostly related to the estimation of the coolant heat capacity, which at low temperatures is high due to the proximity to the critical point. On the other hand, the total power output shows a lower relative change (i.e., <2% points), since it is mostly related to the evolution of the main stream, whose behavior is closer to the ideal one, especially in the second half of the expansion (closer to the outlet conditions). Unlike the power production, the efficiencies, both total-to-total and total-to-static, are affected by the higher estimation of cooling flow, which produces additional losses. Thus, in case the least accurate ideal gas model is used, the sCO_2 turbine performance decreases more than 2% points (i.e., 3.5%) compared to the estimation with the GERG-2008 EoS.

From a geometrical point of view using the ideal gas mixture leads to an underestimation of the mean diameter and blade height at the turbine inlet since the compressibility factor of the CO_2 is around 1.05 at the inlet conditions. The differences in stage size inlet are limited to –0.94% in inlet turbine diameter –2.33% in inlet turbine blade height. On the other hand, the differences in cooling flow requirement are considerable (approximately –42%) mainly due to the significant increase in actual coolant specific heat capacity compared to the ideal gas assumption. In other words, the real-gas behavior of the cooling flows considerably helps in absorbing the heat transferred across the blade. At the turbine outlet, the blade height is approximately 4% higher for the ideal gas assumption because of the larger mass flow rates of cooling flows.

As expected, the increase in the number of stages from 5 to 6 has a positive effect on efficiency. The reason is that each stage has to extract a lower amount of work. Thus, an increase in the number of stages for a given reaction degree, load coefficient, and flow coefficient, implies a lower peripheral speed and a smaller mean diameter. Consequently, the h/D_m ratio becomes higher eventually leading to a reduction of the secondary and tip losses especially in the first and second stages. Figure 7 shows the total-to-total efficiency trend of the various stages for the turbine made by 5 and 6 stages. Note that a reduction of stage count leads to higher fluid-dynamic penalties in the first part of the expansion process. However, due to the lower extraction of work in the hot section of the 6-stage machine, the working fluid remains warmer, and a higher amount of cooling flows is eventually required in the last three stages. The increase of efficiency using a higher number

Table 4 Comparison between the model result of case 1 using two different EoS, the GERG-2008 and the ideal gas mixture

Parameter	Unit of measure	GERG-2008	Ideal gas mixture	Relative difference
Inlet mass flow rate	kg/s	1214.4	1214.4	
Inlet volumetric flow rate	m^3/s	12.04	11.22	–6.79%
Outlet volumetric flow rate	m^3/s	84.81	85.08	+0.32%
Inlet mean diameter	m	0.850	0.842	–0.94%
Outlet mean diameter	m	1.029	1.011	–1.75%
Inlet blade height	m	0.043	0.042	–2.33%
Outlet blade height	m	0.230	0.239	3.91%
Coolant mass flow rate	kg/s	39.17	55.57	+41.86%
Total power output	MW	588.0	578.2	–1.67%
$\eta_{ad,tt}$ total	%	84.65	81.66	–3.53%
$\eta_{ad,ts}$ total	%	81.97	79.19	-3.39%

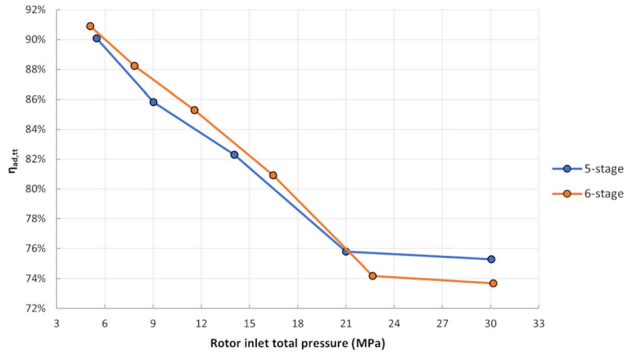

Fig. 7 Total-to-total efficiency of case 2 for both 5- and 6-stage designs and, as a function of the rotor inlet total pressure

of stages ranges between 0.9% and 1.2% points, and it is slightly lower when the load coefficient is lower (i.e., 2.0 instead of 2.5).

The reduction of the load coefficient, i.e., comparing cases 1 and 2, leads to designs with higher mean diameters and peripheral speed, but also with lower flow deflection (flow turning). The reduction of flow deflection is found to positively affect the performance of the stages and the efficiency increase more than counterbalances the decay induced by the smaller ratio between the blade height and the mean diameter, which is especially problematic in the first 1/2 stages. On the other hand, the impact on the cooling requirement deriving from a reduction of work coefficient is rather limited, see Fig. 5. The increase of efficiency using a lower load coefficient is in the range of 0.6–1.2% points, and it is slightly higher when fewer stages are adopted (i.e., 5 instead of 6).

The increase of flow coefficient, i.e., comparing cases 1 and 3, leads to blades with reduced span. This in turn would allow the designer to reduce the blade surface to be cooled and thus the cooling flow requirement. However, this comes at the expense of a lower h/D_m ratio and thus of higher secondary and tip-leakage losses. The efficiency penalty outweighs the performance improvement provided by the decreased cooling requirements, making the choice of high flow coefficient not suited for the optimal design of sCO_2 turbines, especially for the design of the first 1/2 stages. The efficiency penalization by increasing the flow coefficient from 0.6 to 0.9 ranges between 1.8% and 2.6% points. The cases with lower load coefficient, as well as those with fewer stages, are more penalized in terms of efficiency because the h/D_m ratio of the blades increasingly departs from the optimal value of about 1/3.

Table 5 reports the stage total-to-total efficiency as well as the overall total-to-total and total-to-static efficiency of the cases 1–4. It can be seen how the choice of the total number of stages, the load coefficient and the flow coefficient impact the aero-thermal performance of the sCO_2 turbine.

Table 6 compares the h/D_m ratio of the rotor blade. The reported values indicate that, for the case studied, the cooled stages exhibit significantly higher fluid-dynamic losses because of the poor geometrical characteristics in addition to the negative influence of the injection of the coolant. On the other hand, the last stages, not only have less, or no, cooling losses but also better geometrical features, which further increase the efficiency.

The turbine cases labeled with 5–7 are instead designed by discarding the assumption of repeated stages. In other words, the designs are obtained by applying a linear increase of the reaction degree from 0.1 (first stage) to 0.5 (last stage) and a reduction of the load coefficient from 3.0 (first stage) to 1.0 (last stage). A reaction degree of 0.1 at midspan reasonably prevents to reach negative values at the blade root as the free vortex speed distribution would cause, while the value of 0.5 is associated with the maximum fluid-dynamic performance for the stage. Similarly, a work coefficient of 3.0 enables the designer to increase the work extraction in the first stage. The rationale behind this design approach can be summarized as follows: for a cooled turbine, it might be beneficial to rapidly expand the flow in the first 1/2 stages, such to limit the cooling requirements of the overall machine and to enable the design of the last, uncooled, stages with the duty coefficients fixed at their optimal value.

Applying a lower degree of reaction in the design of the first stages does seem to have a weak, albeit positive, impact on both efficiency and cooling flow requirement, see cases 1 and 5. This is

Table 5 Comparison between the stage total-to-static and the total total-to-total and total-to-static efficiency for cases from 1 to 4 and for both the 5- and 6-stage designs.

	$\eta_{ad,tt}$ case 1 (%)		$\eta_{ad,tt}$ case 2 (%)		$\eta_{ad,tt}$ case 3 (%)		$\eta_{ad,tt}$ case 4 (%)	
Stage no.	5 stages	6 stages	5 stages	6 stages	5 stages	6 stages	5 stages	6 stages
1	74.51	72.70	75.29	73.68	73.93	72.72	75.14	73.82
2	75.52	73.96	75.79	74.18	73.94	72.69	74.07	72.47
3	81.70	80.35	82.30	80.92	80.36	79.02	80.66	79.25
4	85.01	84.52	85.83	85.28	84.32	83.69	84.67	83.94
5	89.16	87.30	90.09	88.24	88.95	86.75	89.45	87.22
6		89.97		90.91		89.83		90.34
$\eta_{ad,tt}$ total	84.13	84.65	84.77	85.34	83.29	83.99	83.76	84.36
$\eta_{ad,ts}$ total	81.06	81.97	82.25	83.13	78.94	80.15	79.61	80.71

Table 6 Comparison between the h/D_m ratio of the rotor blade for each stage of cases from 1 to 4 and for both the 5- and 6-stage designs

	h/D_m case 1		h/D_m case 2		h/D_m case 3		h/D_m case 4	
Stage no.	5 stages	6 stages	5 stages	6 stages	5 stages	6 stages	5 stages	6 stages
1	0.05	0.06	0.04	0.05	0.04	0.05	0.03	0.04
2	0.06	0.08	0.04	0.05	0.04	0.05	0.03	0.04
3	0.08	0.09	0.06	0.06	0.06	0.06	0.04	0.05
4	0.11	0.12	0.08	0.08	0.08	0.08	0.06	0.06
5	0.17	0.15	0.12	0.11	0.12	0.11	0.08	0.08
6		0.21		0.15		0.15		0.10

Table 7 Comparison between the stage total-to-static and the total total-to-total and total-to-static efficiency for case 1 and for cases from 5 to 7 and for both the 5- and 6-stage designs

	$\eta_{ad,tt}$ case 1 (%)		$\eta_{ad,tt}$ case 5 (%)		$\eta_{ad,tt}$ case 6 (%)		$\eta_{ad,tt}$ case 7 (%)	
Stage no.	5 stages	6 stages	5 stages	6 stages	5 stages	6 stages	5 stages	6 stages
1	74.51	72.70	73.19	71.05	76.92	75.59	73.55	75.76
2	75.52	73.96	76.99	75.18	77.80	76.34	79.85	78.04
3	81.70	80.35	82.27	80.96	85.16	83.40	86.01	84.06
4	85.01	84.52	85.71	85.10	90.45	88.63	90.89	89.03
5	89.16	87.30	89.47	87.78	93.15	92.14	93.38	92.36
6		89.97		90.19		93.78		93.90
$\eta_{ad,tt}$ total	84.13	84.65	84.46	84.88	85.13	85.54	84.93	86.11
$\eta_{ad,ts}$ total	81.06	81.97	81.36	82.18	83.70	84.29	83.51	84.84

because a low degree of reaction leads to steeper temperature decrease in the first stages of the machine. The overall improvement in the total-to-static efficiency ranges between 0.2% and 0.3% points and it is slightly higher for the 6-stage design.

A substantial positive impact on performance can be obtained by adopting a nonuniform distribution of the work coefficient and making the turbine more front-loaded, i.e., with the first 2 stages having a higher work coefficient than the remaining ones. The advantages of such solution can be clearly observed by comparing cases 1 and 6. For case 1, namely, when the work coefficient has the same value for all the stages (2.5 in case 1), all but the last stage are cooled for both the 5- and 6-stage turbine configuration, while, when the work coefficient is progressively reduced throughout the expansion (from 3.0 to 1.0 in case 6) the second to last rotor does not need cooling in the 5-stage configuration and the second to last stage of the 6-stage configuration does not require any cooling as well. This reasonably suggests that the conventional (for uncooled sCO_2 turbine) design wisdom of repeating stage configuration is not suited for the optimal design of cooled sCO_2 turbines. In case 6, the efficiency of the first 2 stages improves due to both the lower mass flowrate of injected coolant and the higher blade span. On the other hand, the efficiency of the last stages is increased due to the lower work coefficient. The improvement in the performance ranges between 2.3% and 2.6% points.

The benefits of using a combination of nonuniform distribution of reaction degree and load coefficient among the stages are found to be marginal, with only the 6-stages design featuring an efficiency improvement of 0.6% points (case 7 versus case 6), as shown in Table 7.

The results show that the best synchronous cases (i.e., having a rotational speed fixed by the electric grid frequency, i.e., a turbine with a rotational speed of 3600 RPM directly connected to a 60 Hz generator), for both the 5- and 6-stage design, are those with a progressive reduction of the work coefficient, i.e., cases 6 and 7. Figure 8 provides a more in-depth insight into the loss sources of the various rows for the cases 6 and 7 as compared to the baseline case 1. It can be noticed that the fluid-dynamic performance of the last 3 stages for the cases 6 and 7 are higher because of no cooling requirement and reduced profile losses. The reduction of profile losses can be mostly attributed to the lower work coefficient (value of 1) featured by the stages as compared to that of the last 3 stages for the baseline case (value of 2.5). On the other hand, the fluid-dynamic losses of the first 2 stages of cases 6 and 7 are higher compared to those of case 1 especially in the rotor blade of case 7. This is due to the comparatively higher work coefficient of the front stages of turbines 6 and 7. The peak of losses in the 2 and 4 rows (first and second rotor) is instead determined by the low degree of reaction of the first two stages. Overall, it is evident that the cooling requirement of turbines designed at varying work coefficient is lower and therefore such design approach must be preferred in the early design phase of cooled sCO_2 turbines.

4.1 Impact of Rotational Speed on Turbine Design and Performance. The main purpose of using a higher turbine rotational speed is to increase the ratio between the blade span and the mean diameter of the first blade rows, and therefore the efficiency. In order to investigate the impact of the rotational speed on cooled sCO_2 turbine efficiency, the rotational speed is raised from 3600 RPM to 7200 RPM (cases 8 and 9) and the corresponding h/D_m value at the turbine inlet can then be doubled, i.e., from 0.05 to 0.10. The distribution of the duty coefficients among the stages remains instead the same of case 6. The rationale behind this design approach is that high speed machines can be advantageous when the volumetric flowrate is small to increase the h/D_m ratio, which in a synchronous turbine would be small leading to high profile and tip losses. As mentioned above, the first stages of sCO_2 turbines, due to the high density of the working fluid, have small volumetric flowrate also for high power output capacity (order of hundreds of megawatt), thus increasing the rotational speed as well as the h/D_m ratio can have a positive impact on the performance. On the other hand, due to the high volumetric ratio of the machine (ratio between the outlet and inlet volumetric flowrate) the higher h/D_m choice can lead to an unacceptable increase

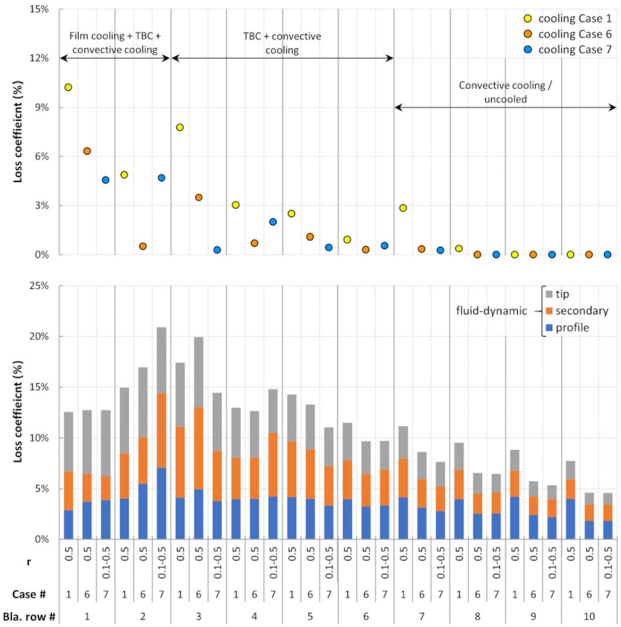

Fig. 8 Comparison of the loss coefficient of cases 1, 6, and 7 for the 5-stage design. In the top section the cooling system loss coefficient and in the bottom section the fluid-dynamic loss coefficient highlighting the contribution of the tip, secondary and profile losses.

Table 8 Comparison between the stage total-to-static and the total total-to-total and total-to-static efficiency of cases 8 and 9. The first one with an axial chord length of 40 mm and a Zweifel coefficient of 0.85, and the second one with an axial chord length of 60 mm and a Zweifel coefficient of 0.65.

Stage no.	$\eta_{ad,tt}$ case 8 (%)	$\eta_{ad,tt}$ case 9 (%)
1	79.61	77.13
2	82.54	80.69
3	87.62	86.91
4	90.77	90.49
5	92.80	92.60
6	93.41	93.17
$\eta_{ad,tt}$ total	89.01	88.05
$\eta_{ad,ts}$ total	85.51	84.64

of the blade aspect ratio of the last stages, which can be balanced by increasing the flow coefficient to 0.9 in order to attain feasible designs. These modifications, significantly reduce the metal surface that has to be cooled, limiting the cooling flow requirement, as shown for case 8 in Fig. 5. Case 8 features an axial chord length of 40 mm and a Zweifel coefficient of 0.85, while case 9 features an axial chord length of 60 mm and a Zweifel coefficient of 0.65, such that the total number of blades in the two cases is comparable. Both designs feature six stages. The increase chord length of case 9 has a negative effect on the coolant requirement, which results to be comparable with that of the synchronous cases, see Fig. 5, since the metal area in contact with the high temperature working fluid increases.

The design obtained by doubling the rotational speed shows that the mean diameter is essentially halved. Despite the efficiency levels are comparatively higher than in the previous cases, and therefore the choice of increasing the rotational speed might seem attractive, there are various challenges associated with that. On the other hand, increasing the rotational speed while keeping a constant ratio between the pitch and the chord length causes a reduction in the blade number (see Eq. (1) with a constant Zweifel coefficient, same chord but lower diameter compared to lower RPM cases). As a consequence, each blade channel elaborates a larger mass flowrate of working fluid thereby increasing the bending stress. Furthermore, the centrifugal force more than doubles due to the blades with higher span and higher rotational speed. Finally, the smaller shaft diameter envisaged for the high-speed turbine causes a major drawback: the transmission of the torque can become problematic, especially for high-power machines, such as the 600 MW one used in the Allam cycle. Indeed, the most stressed section of the rotor shaft is the peripheral one and, since the available space is lower, even if the torque is inversely proportional to the rotational speed, the transmission of the power to the generator can be challenging. Although the higher axial chord length and the suboptimal solidity reduce the fluid-dynamic performance of the turbine, they may be imposed in order to withstand the higher mechanical stress produced by the centrifugal forces compared to the synchronous cases. The overall penalization, as shown in Table 8, is only 0.87% points. Overall, all the results and the considerations point out that a synchronous machine assembly is to be preferred for the design of the cooled sCO_2 turbine of the Allam cycle.

5 Conclusions

In this article, a novel methodology to assess the preliminary thermo-fluid-dynamic performance of sCO_2 turbines and, more generally, cooled expanders using nonconventional working, fluid is presented. The model combines a one-dimensional mean-line code to estimate the preliminary row-by-row geometrical fluid-dynamic design with an extended cooling system model to determine the cooling flow requirement for the blades. The methodology allows the user to select the cooling technology, e.g., convective cooling, film cooling, TBC, or any combination of them, and then computes the amount of cooling flow needed to maintain the blade metal temperature at a selected temperature.

A remarkable advantage of the code is the limited computational time, about 45 s for turbines featuring several stages (e.g., five to six stages), which would allow integrating it with numerical optimization algorithms to find the optimal design variables (rotational speed, number of stages, stage loads, etc.).

The code is applied to preliminary design of the cooled expander of the Allam power cycle. This expander features supercritical inlet conditions (around 1475 K and 30 MPa) and a power output of around 600 MW. The analysis compares several designs differing for the number of stages, 5 or 6, reaction degree, load coefficient, and flow coefficient. The results highlight that:

- Increasing the number of stages allows an efficiency improvement of around 1% point. The performance increase tends to reduce when the load coefficient is lower (i.e., 2.0 instead of 2.5).
- Applying a lower degree of reaction in the design of the first stages does seem to have a positive but weak impact on both efficiency (between 0.2% and 0.3% points) and cooling flow requirement because a low degree of reaction leads to a steeper temperature decrease in the first stages of the machine. A more substantial positive impact on performance can be obtained by adopting a non-uniform distribution of the work coefficient and making the turbine more front-loaded, i.e., with the first two stages having a higher work coefficient than the remaining ones. This suggests that the conventional (for uncooled sCO_2 turbine) design wisdom of repeating stage configuration is not suited for the optimal design of cooled sCO_2 turbines.
- Doubling the rotational speed leads to better fluid-dynamic performance due to the increase of the ratio between blade height and mean diameter (influencing the tip and secondary losses) but several mechanical concerns related to higher bending and centrifugal stresses, and the complication with the mechanical coupling (no reduction gearboxes capable of transmitting such high power are currently commercially available [44]) with the generator may prevent the application to large size turbines.

Hence, a good design of the cooled sCO_2 turbine for the Allam cycle should feature an increasing flow coefficient to match the high increase of the volumetric flowrate of the working fluid, a decreasing load coefficient to produce a fast reduction of the gas temperature in the first stages, reducing the coolant requirement, and a reaction degree close to 0.5 to limit the deflection (flow turning) angle. As a comparison with a conventional gas turbine, even if the film cooling effectiveness is appreciably lower (10% versus 20%), the Allam cycle turbine requires considerably lower coolant flow for the blades. This is because of the higher fluid density causing a considerably smaller ratio of cooled surface per unit of power output (0.15 m^2/MW for a gas turbine, 0.02 m^2/MW for sCO_2 cycle). The lower inlet temperature of gases and cooling flows (thus the high specific heat capacity of the latter) further decreases the cooling flow requirement of the specific turbine design considered in this study.

Future developments of the proposed turbine design model shall include the experimental validation of the heat transfer correlations both for the coolant and main gas side, since the study has shown that the coolant injection can significantly affect the stage thermodynamic performance and verifying that the nondimensional numbers are within the acceptable ranges (i.e., Prandtl > 0.7 and Reynolds $> 10{,}000$), as in this work, may lead to inaccurate results. Thus, the implementation of calibrated correlations would significantly improve the accuracy of the model. A significant future application of the proposed model will feature its integration within a systematic optimization algorithm and the

mechanical/structural analysis of the most critical turbine components aimed at assessing the stresses on the blades and disks.

Nomenclature

Symbols

A = area
a_t = ratio between the gas heat transfer area, including the rotor and case surfaces, and the blade area
c = chord length
c_p = constant pressure heat capacity
C_z = Zweifel load coefficient
D_0 = diameter of the leading edge corresponding cylinder
D_H = hydraulic diameter
D_m = mean diameter
E_f = enhancement factor of the heat transfer process within the cooling channels
h = convective heat transfer coefficient
h_b = blade height
h_t = total enthalpy
I_f = interference factor of the cooling channels
k = thermal conductivity
$\dot{m}$ = mass flow rate
N_b = number of blades
Nu = Nusselt number
p = static pressure
p_b = blade pitch
Pr = Prandtl number
p_t = total pressure
r = reaction degree
Re = Reynolds number
r_{fc} = ratio between the film cooling and total coolant mass flow rates
r_m = mean radius
s = entropy
t = thickness
T = static temperature
T_{aw} = adiabatic blade wall temperature
T_{bmax} = maximum allowed blade wall temperature
v = absolute velocity magnitude
W = molecular mass
$\dot{W}$ = power
x = linear coordinate along the pressure and suction side corresponding flat surface

Greek Symbols

α = absolute velocity angle
α_{ic} = relative coolant injection angle
Δ = property variation
η = overall cooling effectiveness
η_{ad} = adiabatic efficiency
η_{fc} = film cooling effectiveness
ϑ = tangential coordinate of the leading edge corresponding cylinder
λ = ratio between the gas heat transfer area, including the rotor and case surfaces, and the mean cross-sectional area throughout the gas is flowing
μ = dynamic viscosity
ξ = ratio between the coolant and main stream mass flow rates
ρ = static density
σ = blade solidity
φ = flow coefficient
Ψ_g = parameter accounting for the reduction of the gas cross-sectional area due to the blade thickness
ψ = load coefficient

Subscripts

a = axial
bw = blade wall
c = coolant/cooling channel
g = main gas stream
gf = gas property at the film cooling conditions
i = inlet property
o = outlet property
oc = property at the blade row outlet before the mixing with the convective cooling coolant stream
ouc = property at the blade row outlet for the uncooled expansion
t = tangential
TBC = thermal barrier coating layer
ts = total-to-static
tt = total-to-total
x = property along the linear coordinate of the pressure and suction side corresponding flat surface
ϑ = property along the tangential coordinate of the leading edge corresponding cylinder
∞ = approaching property

Acronyms

CFD = computational fluid dynamics
EoS = equation of state
GS = gas-steam cycles software [22,30]
IEA-GHG = International Energy Agency Greenhouse Gas R&D Program
OEM = original equipment manufacturer
TBC = thermal barrier coating
TOT = turbine outlet temperature

Appendix

The cooling flow requirement of a blade cascade and the related efficiency penalty is determined through an iterative computational procedure which is shown in Fig. 9. The iteration variables are the overall cooling effectiveness (η) and the ratio between the

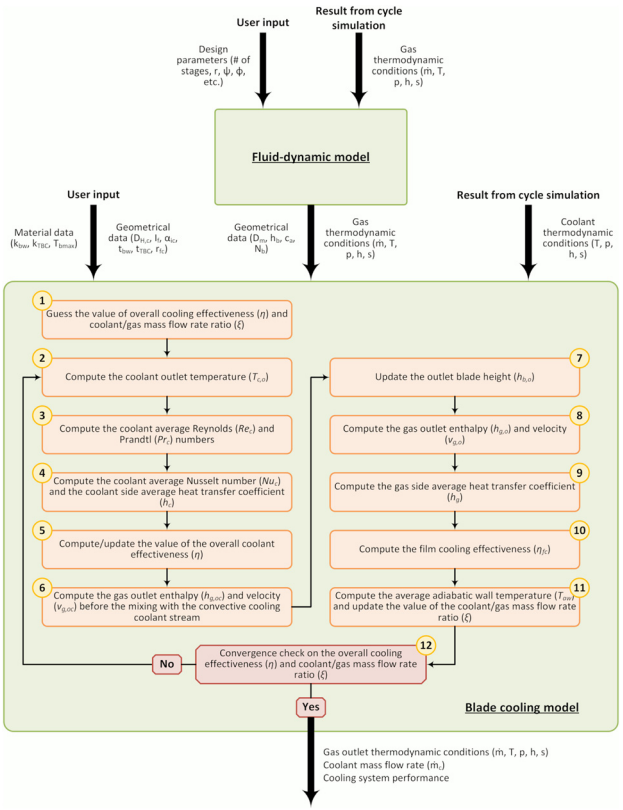

Fig. 9 Block flow diagram of the iterative computational procedure of the cooling system model. The numbers of the computational steps refer to the description list in the text.

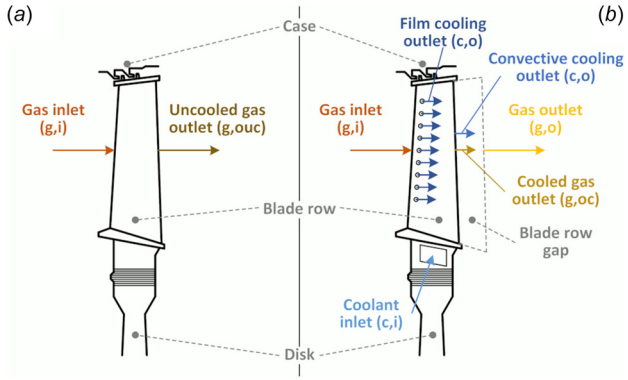

Fig. 10 Simplified scheme of the expansion model for a single blade row. On the left-hand side (*a*) the uncooled expansion, and on the right-hand side (*b*) the cooled case. Each stream is labeled and in the brackets is reported the subscript of the thermo-physical properties as used in the equations.

coolant mass flowrate and that of the main stream (ξ). The computation procedure is here described for the most general case, in which convective, film cooling, and TBC all along the blade surface are used. However, the same methodology can be applied to simpler cooling system configurations where, for instance, TBC and/or film cooling are not applied. Figure 10 shows the nomenclature associated with the flow streams in a blade cascade for the case of no blade cooling, on the left-hand side, and with cooling, on the right-hand side. For each stream, the figure also reports between brackets the corresponding subscript of thermo-physical properties as used in the equations.

The iterative calculation procedure is as follows:

(1) First, for each turbine stage, the need for blade cooling is assessed by comparing the inlet recovery temperature [45] of the main stream with the maximum metal temperature set by the user. If the recovery temperature is lower, no cooling is required. Otherwise, an initial value for the overall cooling effectiveness (η) and the ratio between the coolant mass flow rate and that of the main stream (ξ) is guessed.

(2) Given the inlet temperature of the coolant ($T_{c,i}$) provided by the user (which comes from cycle calculations), a first estimate of the coolant outlet temperature ($T_{c,o}$) is determined using the definition of the overall cooling effectiveness in Eq. (A1).

$$T_{c,o} = T_{c,i} + \eta(T_{bmax} - T_{c,i}) \tag{A1}$$

(3) Hence, it is possible to evaluate the average thermodynamic properties of the coolant and thereby computing the Reynolds (Re_c) and Prandtl (Pr_c) numbers within the cooling channels.

(4) Then, the Dittus–Bolter correlation [28], which is able to correctly describe low temperature CO_2 streams [46], reported in Eq. (A2), is used to determine the average Nusselt (Nu_c) number and, with Eq. (A3), the coolant heat transfer coefficient (h_c). The factor E_f is introduced in Eq. (A2) to account for the ribs and internal channel geometry (e.g., impingement) adopted to enhance the heat transfer coefficient of the cooling flow. In this work it is assumed that $E_f = 2.5$ [27]

$$Nu_c = E_f Re_c^{0.8} Pr_c^{0.4} \tag{A2}$$

$$h_c = Nu_c \frac{k_c}{D_{H,c}} \tag{A3}$$

(5) Since the external wall temperature of the blade is a fixed parameter of the model, a new value for the overall cooling effectiveness can be estimated using Eq. (A4)

$$\eta = 1 - \exp\{-NTU\} = 1 - \exp\left\{\frac{\left(\frac{1}{h_c} + \frac{t_{bw}}{k_{bw}}\right)^{-1} I_f A_c}{\frac{\dot{m}_c \Delta h_{t,c}}{T_{c,o} - T_{c,i}}}\right\} \tag{A4}$$

where the coolant mass flow rate ($\dot{m}_c$) is computed given the initial guess for the ratio between the gas and coolant mass flow rates (ξ) and $\Delta h_{t,c}$ is the total enthalpy rise in the coolant at the channel outlet (the inlet enthalpy is an input variable of the model, derived from the cycle simulation, and the outlet enthalpy is computed at point 3). The product of $\dot{m}_c$ and $\Delta h_{t,c}$ represents the thermal power transferred through the blade wall. The heat transfer area of the cooling channels (A_c) is corrected with an interference factor (I_f) to account for the surface between adjacent channels, which does not absorb heat from the blade external wall, but it is heated only through a heat conduction process. The interference factor value can be selected by the user for each blade row and typical vales are in the range 0.6–0.8, and 0.75 has been selected for the case study of this work.

(6) The thermodynamic conditions of the expanding gas resulting from the mixing of the bulk flow with the film cooling are computed by applying the energy and momentum balance, Eqs. (A5) and (A6), respectively

$$\dot{m}_g h_{t,g,i} + r_{fc}\dot{m}_c h_{t,c,o} = (\dot{m}_g + r_{fc}\dot{m}_c) h_{t,g,oc} + \dot{m}_c \Delta h_{t,c} \tag{A5}$$

$$\left(\frac{p_{g,ouc}}{\rho_{g,ouc} v_{g,ouc}} + v_{g,ouc}\right)\dot{m}_g + r_{fc}\dot{m}_c v_{c,o}\cos(\alpha_{ic}) = \left(\frac{p_{g,oc}}{\rho_{g,oc} v_{g,oc}} + v_{g,oc}\right)(\dot{m}_g + r_{fc}\dot{m}_c) \tag{A6}$$

The gas total enthalpy at outlet ($h_{t,g,oc}$) results from the mixing of the gas bulk flow ($\dot{m}_g$) with the film cooling stream ($r_{fc}\dot{m}_c$), as well as the convective heat transfer across the blade wall ($\dot{m}_c \Delta h_{t,c}$). The control volume considered by the energy balance is the blade flow passage (i.e., region between two adjacent blades in Fig. 3); then, Eq. (A5) does not account for the contribution due to the convective cooling flow.The momentum balance (Eq. (A6) allows the computation of the outlet velocity after the mixing process, and the performance penalty related to blade cooling, quantified by the reduction of the total thermodynamic condition considering a fixed static outlet pressure. The equation is written assuming that a mixing process occurs at the exit of the blade row, between the hot gas going through an equivalent uncooled blade cascade (subscript ouc) and the cooling stream. Their mixing results in the cooled gas stream (subscript oc), for which the total enthalpy has been determined by means of the energy balance in Eq. (A5). This approximation allows for computing the fluid-dynamic losses associated with film cooling. Since we assume that the gas velocity does not change direction during the mixing process, the momentum balance accounts only for the terms along the bulk flow direction. Conversely, the component of the coolant velocity perpendicular to the direction of the bulk flow is assumed to be completely dissipated.

(7) The outlet blade span is computed with Eq. (A7) considering that the outlet conditions differ from the uncooled case. As a result of the cooling process, the fluid outlet density is higher and, due to the mixing process, the outlet mass flow rate is higher, while the absolute velocity magnitude is lower

$$\dot{m}_g + r_{fc}\dot{m}_c = \pi D_{m,o} h_{b,o} v_{g,oc} \cos(\alpha_o) \rho_{g,oc} \tag{A7}$$

(8) The thermodynamic conditions at the cascade outlet are calculated based on the energy balance, see Eq. (A8), and the momentum balance of Eq. (A9). With respect to Eq. (A5), the control volume considered to derive Eq. (A8) encompasses the whole blade row (no heat transfer term appears, because the heat transfer surface, i.e., the blade wall, is not at the boundary, but it is completely within the control volume). Conversely, the momentum balance, Eq. (A9), is written according to a control volume encompassing only the blade row gap, where the gas exiting the blade row (subscript oc) mixes with the convective cooling stream ($1 - r_{fc}$). The estimated thermodynamic conditions at the cascade outlet represent, then, the input for the next blade row computation

$$\dot{m}_g h_{t,g,i} + \dot{m}_c h_{t,c,i} = (\dot{m}_g + \dot{m}_c) h_{t,g,o} \tag{A8}$$

$$\left(\frac{p_{g,oc}}{\rho_{g,oc} v_{g,oc}} + v_{g,oc}\right)\dot{m}_g + (1 - r_{fc})\dot{m}_c v_{c,o}\cos(\alpha_{ic}) = \left(\frac{p_{g,o}}{\rho_{g,o} v_{g,o}} + v_{g,o}\right)(\dot{m}_g + (1 - r_{fc})\dot{m}_c) \tag{A9}$$

Once the blade row outlet mass flow rate and velocity are known, the blade span at the next row inlet is computed applying the continuity equation and assuming that the mean diameter does not change (i.e., it is equal to the value at the outlet of the previous row).

(9) When both the thermodynamic conditions at the inlet and outlet of a blade cascade are known, the convective heat transfer coefficient on the gas side can be calculated. According to the method of Simon and Piggush [27], the blade profile is divided in two sections. The leading edge is modeled as a crossflow cylinder, and Eq. (A10) is used to compute the mean integral value of the heat transfer coefficient (h_ϑ) along the tangential coordinate (ϑ) of the cylinder

$$\frac{h_\vartheta D_0}{k_g} = 1.14\left(\frac{\rho_g v_\infty D_0}{\mu_g}\right)^{0.5} \mathrm{Pr}_g^{0.4}\left[1 - \left(\frac{\vartheta}{90}\right)^3\right] \tag{A10}$$

The pressure and suction sides are, instead, modeled as flat surfaces, and Eq. (A11) is used to determine the mean integral value of the heat transfer coefficient (h_x) along the flow direction (x)

$$\frac{h_x}{\rho_g c_{p,g} v_\infty} = 0.0296\mathrm{Re}_x^{-0.2}\mathrm{Pr}_g^{-2/3} \tag{A11}$$

Both Eqs. (A10) and (A11) are proposed by Simon and Piggush [27], and the overall convective heat transfer coefficient of the blade is obtained by averaging h_x and h_ϑ with weight w_x and w_ϑ, whose values are, respectively, 0.869 and 0.131 derived using the integration limit proposed in [27] of 1.40 rad (80 degree) for the leading edge equation. The value for the two weights has been derived for the simplified blade geometry (cylinder and flat surfaces) using the conservative integration boundaries proposed by Simon and Piggush [27].

(10) The inlet and outlet film cooling temperatures are computed accordingly to Goldstein et al. [47]. Then, it is possible to calculate the gas properties of the film region (subscript gf) and an equivalent effectiveness for film cooling (η_{fc}) according to the semi-empirical correlation proposed by Goldstein and Haji-Sheikh [48], which reads

$$\eta_{fc} = \frac{1.9\mathrm{Pr}_{gf}^{2/3}}{1 + 0.329\frac{c_{p,gf}}{c_{p,c}}\mathrm{Re}_{gf}^{-0.2}\left(\frac{x}{c}\right)^{0.8}\left[\frac{2a_t\sigma}{\Psi_g}\frac{\dot{m}_g}{r_{fc}\dot{m}_c} + 0.00015\mathrm{Re}_{gf}\frac{W_g}{W_c}\sin(\alpha_{ic})\right]} \tag{A12}$$

where a_t is the ratio between the gas heat transfer area, including the rotor and case surfaces, and the blade area, σ is the solidity, and Ψ_g is a parameter accounting for the reduction of the gas cross-sectional area due to the blade thickness.

(11) The value of the film cooling effectiveness calculated from Eq. (A12) is then used to compute leading- and trailing-edge adiabatic wall temperature, as from Eq. (A13). The average value of T_{aw} is used to calculate a new value for the ratio between the coolant and the inlet gas mass flow rates (ξ) according to the energy balance of the heat transfer process across the blade, as in Eq. (A14). Note that λ is the ratio between the gas heat transfer area (including the rotor and case surfaces) and the mean cross-sectional area of the blade channel

$$T_{aw} = T_g - \eta_{fc}(T_g - T_{c,o}) \tag{A13}$$

$$\xi = \lambda\left(\frac{1}{h_g} + \frac{t_{TBC}}{k_{TBC}}\right)^{-1}\frac{1}{\rho_g v_{g,o}}\frac{T_{aw} - T_{bmax}}{\Delta h_{t,c}} \tag{A14}$$

(12) At this point, both the initially guessed values of the overall cooling effectiveness (η) and the ratio between the coolant and inlet gas mass flow rates (ξ), have been updated, respectively with Eqs. (A4) and (A14). The iterative procedure is repeated, starting from point 2, and solved with the direct substitution method, until the convergence on the relative error of the two variables is below a given threshold (10^{-6}).

The methodology discussed above is applied to the rotor blade rows with the following modifications: the relative velocities replace the absolute ones, the total-relative properties substitute the total-absolute ones, and the rothalpy replaces the total enthalpy.

Note, finally, that the model does not allow the designer to estimate the cooling flow requirement for the disks and the casing, which, in a conventional gas turbine, accounts for around one percent of the inlet gas flowrate for each cooled stage [30]. However, as the sCO_2 turbine is expected to be much more compact than a conventional gas turbine of the same power capacity, it is envisaged that the disks and the casing cooling demand will be lower. This expected result derives from the fact that the material constituting the case and disks act as a fin extracting thermal power from other pieces of metal in direct contact with the hot gas. Thus, since the high density of the working fluid leads to smaller case and disks, the heat dissipated is required to be removed to avoid excessive temperature, from the material is lower compared to conventional gas turbines.

References

[1] Alsagri, A. S., Chiasson, A., and Gadalla, M., 2019, "Viability Assessment of a Concentrated Solar Power Tower With a Supercritical CO_2 Brayton Cycle Power Plant," ASME J. Sol. Energy Eng., **141**(5), p. 051006.

[2] Moore, J., Brun, K., Evans, N., and Kalra, C., 2015, "Development of 1 MWe Supercritical CO_2 Test Loop," ASME Paper No. GT2015-43771.

[3] Dostal, V., Driscoll, M. J., Hejzlar, P., and Todreas, N. E., 2002, "A Supercritical CO_2 Gas Turbine Power Cycle for Next-Generation Nuclear Reactors," ASME Paper No. ICONE10-22192.

[4] Marion, J., Kutin, M., McClung, A., Mortzheim, J., and Ames, R., 2019, "The STEP 10 MWe sCO_2 Pilot Plant Demonstration," ASME Paper No. GT2019-91917.

[5] Thanganadar, D., Asfand, F., and Patchigolla, K., 2019, "Thermal Performance and Economic Analysis of Supercritical Carbon Dioxide Cycles in Combined Cycle Power Plant," Appl. Energy, **255**, p. 113836.

[6] Bolland, O., and Mathieu, P., 1998, "Comparison of Two CO_2 Removal Options in Combined Cycle Power Plants," Energy Convers. Manag., **39**(16–18), pp. 1653–1663.

[7] Rao, A. D., 2012, Combined Cycle Systems for Near-Zero Emission Power Generation, Woodhead Publishing, Oxford, UK.

[8] International Energy Agency Greenhouse Gas R&D Programme (IEAGHG), 2015, "Oxy-Combustion Turbine Power Plants," IEAGHG, Cheltenham, UK, accessed Sept. 1, 2021, https://ieaghg.org/docs/General_Docs/Reports/2015-05.pdf

[9] Scaccabarozzi, R., Gatti, M., and Martelli, E., 2016, "Thermodynamic Analysis and Numerical Optimization of the NET Power Oxy-Combustion Cycle," Appl. Energy, **178**, pp. 505–526.
[10] Zaryab, S. A., Scaccabarozzi, R., and Martelli, E., 2020, "Advanced Part-Load Control Strategies for the Allam Cycle," Appl. Therm. Eng., **168**, p. 114822.
[11] Scaccabarozzi, R., Gatti, M., and Martelli, E., 2017, "Thermodynamic Optimization and Part-Load Analysis of the NET Power Cycle," Energy Procedia, **114**, pp. 551–560.
[12] Ferrari, N., Mancuso, L., Davison, J., Chiesa, P., Martelli, E., and Romano, M. C., 2017, "Oxy-Turbine for Power Plant With CO_2 Capture," Energy Procedia, **114**, pp. 471–480.
[13] Allam, R. J., Palmer, M. R., Brown, G. W., Fetvedt, J. E., Freed, D. A., Nomoto, H., Itoh, M., Okita, N., and Jones, C., 2013, "High Efficiency and Low Cost of Electricity Generation From Fossil Fuels While Eliminating Atmospheric Emissions, Including Carbon Dioxide," Energy Procedia, **37**, pp. 1135–1149.
[14] Allam, R., Martin, S., Forrest, B., Fetvedt, J., Lu, X., Freed, D., Brown, G. W., Sasaki, T., Itoh, M., and Manning, J., 2017, "Demonstration of the Allam Cycle: An Update on the Development Status of a High Efficiency Supercritical Carbon Dioxide Power Process Employing Full Carbon Capture," Energy Procedia, **114**, pp. 5948–5966.
[15] Moroz, L., Frolov, B., Burlaka, M., and Guriev, O., 2014, "Turbomachinery Flowpath Design and Performance Analysis for Supercritical CO_2," ASME Paper No. GT2014-25385.
[16] Zhang, H., Zhao, H., Deng, Q., and Feng, Z., 2015, "Aerothermodynamic Design and Numerical Investigation of Supercritical Carbon Dioxide Turbine," ASME Paper No. GT2015-42619.
[17] Wright, I. G., Pint, B. A., Shingledecker, J. P., and Thimsen, D., 2013, "Materials Considerations for Supercritical CO_2 Turbine Cycles," ASME Paper No. GT2013-94941.
[18] Sasaki, T., Itoh, M., Maeda, H., Tominaga, J., Saito, D., and Niizeki, Y., 2017, "Development of Turbine and Combustor for a Semi-Closed Recuperated Brayton Cycle of Supercritical Carbon Dioxide," ASME Paper No. POWER-ICOPE2017-3419.
[19] Han, W., Zhang, Y., Li, H., Yao, M., Wang, Y., Feng, Z., Zhou, D., and Dan, G., 2019, "Aerodynamic Design of the High Pressure and Low Pressure Axial Turbines for the Improved Coal-Fired Recompression SCO_2 Reheated Brayton Cycle," Energy, **179**, pp. 442–453.
[20] Schmitt, J., Willis, R., Amos, D., Kapat, J., and Custer, C., 2014, "Study of a Supercritical CO_2 Turbine With TIT of 1350 K for Brayton Cycle With 100 MW Class Output: Aerodynamic Analysis of Stage 1 Vane," ASME Paper No. GT2014-27214.
[21] Denton, J. D., 1993, "The 1993 IGTI Scholar Lecture: Loss Mechanisms in Turbomachines," ASME J. Turbomach., **115**(4), pp. 621–656.
[22] Consonni, S., 1992, "Performance Prediction of Gas/Steam Cycles for Power Generation," Ph.D. thesis, No. 1893-T, Princeton University, Princeton, NJ.
[23] El-Masri, M. A., 1986, "On Thermodynamics of Gas-Turbine Cycles: Part 2—A Model for Expansion in Cooled Turbines," ASME J. Eng. Gas Turbines Power, **108**(1), pp. 151–159.
[24] Horlock, J. H., Watson, D. T., and Jones, T. V., 2001, "Limitations on Gas Turbine Performance Imposed by Large Turbine Cooling Flows," ASME J. Eng. Gas Turbines Power, **123**(3), pp. 487–494.
[25] Torbidoni, L., and Massardo, A. F., 2004, "Analytical Blade Row Cooling Model for Innovative Gas Turbine Cycle Evaluations Supported by Semi-Empirical Air-Cooled Blade Data," ASME J. Eng. Gas Turbines Power, **126**(3), pp. 498–506.
[26] Traupel, W., 1982, *Thermische Turbomaschinen*, Springer Berlin Heidelberg, Berlin, Heidelberg, Germany.
[27] Simon, T., and Piggush, J., 2008, "Hot Gas Path Heat Transfer Characteristics/Active Cooling of Turbine Components," *Thermal Engineering in Power Systems*, R. S. Amano, and B. Sundén, eds., WIT Press, Ashurst, Southampton, UK, pp. 231–303.
[28] Dittus, F. W., and Boelter, L. M. K., 1985, "Heat Transfer in Automobile Radiators of the Tubular Type," Int. Commun. Heat Mass Trans., **12**(1), pp. 3–22.
[29] El-Masri, M. A., 1988, "GASCAN—An Interactive Code for Thermal Analysis of Gas Turbine Systems," ASME J. Eng. Gas Turbines Power, **110**(2), pp. 201–209.
[30] Chiesa, P., and Macchi, E., 2004, "A Thermodynamic Analysis of Different Options to Break 60% Electric Efficiency in Combined Cycle Power Plants," ASME J. Eng. Gas Turbines Power, **126**(4), pp. 770–785.
[31] Jordal, K., Torbidoni, L., and Massardo, A. F., 2001, "Convective Blade Cooling Modelling for the Analysis of Innovative Gas Turbine Cycles," ASME Paper No. 2001-GT-0390.
[32] Pini, M., Persico, G., Casati, E., and Dossena, V., 2013, "Preliminary Design of a Centrifugal Turbine for Organic Rankine Cycle Applications," ASME J. Eng. Gas Turbines Power, **135**(4), p. 042312.
[33] Bahamonde, S., Pini, M., De Servi, C., Rubino, A., and Colonna, P., 2017, "Method for the Preliminary Fluid Dynamic Design of High-Temperature Mini-Organic Rankine Cycle Turbines," ASME J. Eng. Gas Turbines Power, **139**(8), p. 082606.
[34] Colonna, P., van der Stelt, T., and Guardone, A. M. A., 2012, "FluidProp (Version 3.0): a Program for the Estimation of Thermophysical Properties of Fluids," Asimptote, Delft, The Netherlands, accessed Sept. 1, 2021, http://www.asimptote.nl/software/fluidprop
[35] Kunz, O., and Wagner, W., 2012, "The GERG-2008 Wide-Range Equation of State for Natural Gases and Other Mixtures: An Expansion of GERG-2004," J. Chem. Eng. Data, **57**(11), pp. 3032–3091.
[36] Zweifel, O., 1945, "The Spacing of Turbo-Machine Blading Especially With Large Angular Deflection," Brown Boveri Rev., **32**(1), pp. 436–444.
[37] Gülen, S. C., 2019, *Gas Turbines for Electric Power Generation*, Cambridge University Press, Cambridge, UK.
[38] Unglaube, T., and Chiang, H.-W. D., 2020, "Preliminary Design of Small-Scale Supercritical CO_2 Radial Inflow Turbines," ASME J. Eng. Gas Turbines Power, **142**(2), p. 021011.
[39] Scaccabarozzi, R., Martelli, E., Gatti, M., Chiesa, P., Pini, M., and De Servi, C., 2019, "Conceptual Thermo-Fluid Dynamic Design of the Cooled Supercritical CO_2 Turbine for the Allam Cycle," International Conference on Applied Energy, Vol. 5, Västerås, Sweden, Aug. 12–15, p. 1047.
[40] Moustapha, S. H., Okapuu, U., and Williamson, R. G., 1987, "Influence of Rotor Blade Aerodynamic Loading on the Performance of a Highly Loaded Turbine Stage," ASME J. Turbomach., **109**(2), pp. 155–161.
[41] Willinger, R., and Haselbacher, H., 1998, "The Role of Rotor Tip Clearance on the Aerodynamic Interaction of a Last Gas Turbine Stage and an Exhaust Diffuser," ASME Paper No. 98-GT-094.
[42] Dixon, S. L., and Hall, C., 2014, *Fluid Mechanics and Thermodynamics of Turbomachinery*, 7th ed., Butterworth-Heinemann, Oxford, UK.
[43] Gyftopoulos, E. P., and Beretta, G. P., 2005, *Thermodynamics: Foundations and Applications*, New York.
[44] Bidkar, R. A., Mann, A., Singh, R., Sevincer, E., Cich, S., Day, M., Kulhanek, C. D., Thatte, A. M., Peter, A. M., Hofer, D., and Moore, J., 2016, "Conceptual Designs of 50 MWe and 450 MWe Supercritical CO_2 Turbomachinery Trains for Power Generation From Coal. Part 1: Cycle and Turbine," Fifth International Symposium—Supercritical CO_2 Power Cycles, San Antonio, Texas, Mar. 28–31.
[45] Holman, J. P., 2009, *Heat Transfer*, 10th ed., McGraw-Hill, New York.
[46] van Eldik, M., Harris, P. M., Kaiser, W. H., and Rousseau, P. G., 2014, "Theoretical and Experimental Analysis of Supercritical Carbon Dioxide Cooling," International Refrigeration and Air Conditioning Conference, Purdue e-Pubs, Purdue University, West Lafayette, IN, July 14–17, p. 2113.
[47] Goldstein, R. J., Eckert, E. R. G., and Wilson, D. J., 1968, "Film Cooling With Normal Injection Into a Supersonic Flow," ASME J. Eng. Ind., **90**(4), pp. 584–588.
[48] Goldstein, R. J., and Haji-Sheikh, A., 1967, "Prediction of Film Cooling Effectiveness," Proceedings of JSME 1967 Semi-International Symposium, Tokyo, Japan, Sept. 4–8, pp. 213–218.